



저작자표시-비영리-변경금지 2.0 대한민국

이용자는 아래의 조건을 따르는 경우에 한하여 자유롭게

- 이 저작물을 복제, 배포, 전송, 전시, 공연 및 방송할 수 있습니다.

다음과 같은 조건을 따라야 합니다:



저작자표시. 귀하는 원저작자를 표시하여야 합니다.



비영리. 귀하는 이 저작물을 영리 목적으로 이용할 수 없습니다.



변경금지. 귀하는 이 저작물을 개작, 변형 또는 가공할 수 없습니다.

- 귀하는, 이 저작물의 재이용이나 배포의 경우, 이 저작물에 적용된 이용허락조건을 명확하게 나타내어야 합니다.
- 저작권자로부터 별도의 허가를 받으면 이러한 조건들은 적용되지 않습니다.

저작권법에 따른 이용자의 권리는 위의 내용에 의하여 영향을 받지 않습니다.

이것은 [이용허락규약\(Legal Code\)](#)을 이해하기 쉽게 요약한 것입니다.

[Disclaimer](#)

보건학석사학위논문

**Degradation Mechanisms of
Microcystin-LR during UV-B
Photolysis and UV-B/H₂O₂ Processes:
By-products and Pathways**

자외선 광분해와 자외선/과산화수소 과정을 이용한
마이크로시스틴-LR의 분해 메커니즘 연구:
부산물과 분해경로에 대하여

2016년 8월

서울대학교 보건대학원

환경보건학과 환경보건학 전공

문보람

Contents

Abstract.....	i
List of Figures.....	iii
List of Tables.....	v
1. Introduction.....	1
1.1.....	1
1.2.....	8
1.3.....	11
2. Materials and Methods.....	11
2.1.....	11
2.2.....	13
2.3.....	16
3. Results and Discussion.....	20
3.1.....	20
3.2.....	25
3.3.....	28
3.4.....	36
4. Conclusions.....	45
5. References.....	46
국문초록.....	53

Abstract

In recent years, the increasing intensity and frequency of algal blooms in surface water has become a serious problem. The most common toxins produced by cyanobacteria are microcystins (MCs), which are reported to be cyclic heptapeptides. In particular, microcystin-LR (MC-LR) has been found to be one of the most abundant and toxic compounds. Therefore, the presence of MC-LR in water sources is of concern due to its direct threats to human health in finished water. In order to remove the MC-LR, the removals of MC-LR by chlorination, ozonation, and UV/AOPs have been widely reported, but only a little were investigated on the formation of their by-products during water treatment techniques. Therefore, the investigation of MC-LR by-products formed during treatment processes needed. In this study, removal and degradation pathways of MC-LR (m/z 995.6) were examined during UV-B photolysis and UV-B/H₂O₂ processes based on the identification of by-products using liquid chromatography–tandem mass spectrometry (LC-MS/MS). The UV-B/H₂O₂ process was more efficient than UV-B photolysis for MC-LR removal. While eight by-products were newly identified during UV-B photolysis (m/z 414.3, 417.3, 709.6, 428.9, 608.6, 847.5, 807.4, and 823.6), eleven by-products were newly confirmed during the UV-B/H₂O₂ process (m/z 707.4, 414.7, 429.3, 445.3, 608.6, 1052.0, 313.4, 823.6, 357.3, 245.2, and 805.7). Most MC-LR by-products had lower m/z than MC-LR during two processes. Based on the identified by-products and their peak area patterns,

potential degradation mechanisms during the two processes were proposed. While bond cleavage and free electron pair transfer reactions containing nitrogen atoms were the major reactions during UV-B photolysis, the reaction with an OH radical and addition reaction with other by-products were identified as additional reaction pathways during the UV-B/H₂O₂ process.

Keywords: Microcystin-LR; UV-B photolysis; UV-B/H₂O₂; by-products; degradation pathway

Student Number: 2014-23351

List of Figures

Figure. 1. Schematic diagram of a photolytic reactor.....	15
Figure. 2. LC-MS/MS chromatograms of MC-LR (retention time: 3.67 min; $r^2=0.9997$).....	19
Figure. 3. Removal of microcystin-LR (MC-LR) during the UV-B photolysis and UV-B/H ₂ O ₂ processes at different UV intensities: (a) 0.47, (b) 0.58, and (c) 1.57 mW/cm ² (n = 2, [C ₀] = 100 µg/L, [H ₂ O ₂] = 1 mg/L, 20°C).....	22
Figure. 4. Effect of UV intensity (a) and H ₂ O ₂ dose (b) (n = 2, [C ₀] = 100 µg/L, UV intensity = 0.47, 0.58, and 1.57 mW/cm ² , [H ₂ O ₂] = 1, 2, and 4 mg/L, 20°C).....	23
Figure. 5. Time profiles of the degradation by-products during UV-B photolysis ([C ₀] = 100 µg/L, UV intensity = 5.74 mW/cm ² , 20°C, reaction time = 6 h).....	33
Figure. 6. Time profiles of the degradation by-products by UV-B/H ₂ O ₂ process ([C ₀] = 100 µg/L, [H ₂ O ₂] = 1 mg/L, UV intensity = 5.68 mW/cm ² , 20°C, reaction time = 24 h).....	34

Figure. 7. Time profiles of each by-product by UV-B/H ₂ O ₂ process ([C ₀] = 100 µg/L, [H ₂ O ₂] = 1 mg/L, UV intensity = 5.68 mW/cm ² , 20°C, reaction time = 24 h).....	35
Figure. 8. Proposed MC-LR degradation pathways for UV-B photolysis.....	39
Figure. 9. Proposed MC-LR degradation pathways for the UV-B/H ₂ O ₂ process.....	43
Figure. 10. Changes in accumulated peak area for the identified by-products during the UV-B/H ₂ O ₂ process with a H ₂ O ₂ dose of (a) 1 mg/L or (b) 4 mg/L ([C ₀] = 100 µg/L, UV intensity = 5.68 mW/cm ² , 20°C, reaction time = 6 h).....	44

List of Tables

Table. 1. The guideline of MCs in drinking water.....	3
Table. 2. The guideline of MCs in recreational water.....	4
Table. 3. Worldwide occurrence of MC-LR in water.....	5
Table. 4. Physicochemical properties of MC-LR.....	12
Table. 5. Optimized LC-MS/MS condition for the analysis of MC-L.....	18
Table. 6. Changes in rate constants (k) and R^2 by adjusting the UV intensity and H_2O_2 dose during the UV-B photolysis and UV-B/ H_2O_2 processes.....	24
Table. 7. Fragmentation results for MC-LR degradation by-products during the UV-B photolysis and UV-B/ H_2O_2 processes.....	27
Table. 8. Optimized LC-MS/MS conditions for the analysis of MC-LR and its by-products during UV-B photolysis.....	31

Table. 9. Optimized LC-MS/MS conditions for the analysis of MC-LR and its by-products during UV-B/H ₂ O ₂ process.....	32
--	----

1. Introduction

1.1. Background

In recent years, the increasing intensity and frequency of algal blooms in surface water has become a serious problem. The most common toxins produced by cyanobacteria are microcystins (MCs), which are reported to be cyclic heptapeptides. Among the more than 100 microcystin isoform structures identified (Feurstein et al. (2011)), microcystin-LR (MC-LR) has been found to be one of the toxic compounds (Rinehart et al. (1994)). MC-LR consists of a cyclic heptapeptide and a side chain of 3-amino-9-methoxy-2,6,8-trimethyl-10-phenyl-4,6-decadienoic acid (ADDA) is one of the seven amino acids of the heptapeptide. Its toxicity corresponds with the conjugated diene on the ADDA side chain (An et al. (1994)). It is reported that degradation by-products containing the ADDA functional group can still possess a certain level of biological toxicity (Zong et al. (2013)).

The presence of MC-LR in water sources is of concern due to its direct threats to human health in finished water. The primary target organ for MC-LR is the liver. MC-LR inhibits protein phosphatase type 1 and 2A activities in the cytoplasm of liver cells (Weng et al. (2007)). According to the International Agency for Research on Cancer (IARC), MC-LR is possibly carcinogenic to humans (Group 2B). The US

Environmental Protection Agency (EPA) has reported health effects of MC-LR exposure including vomiting, diarrhea, liver inflammation, acute pneumonia, kidney damage, and the potential promotion of tumour growth (US EPA (2012)). MC-LR also has negative effects on the endocrine system in females (Zhao et al. (2015)). For this reason, many countries issued a guideline for MCs in drinking and recreational water (Table 1-2). There are previous researches which are the analyses of the concentration of MC-LR in water system. Table 1 summarizes worldwide occurrence of MC-LR in water. As shown Table 3, the MC-LR concentrations varied from N.D. to 2,100 µg/L. The presence of these levels of MC-LR in water may cause health effects in humans.

Table. 1. The guideline of MCs in drinking water

Country	Guideline (µg/L)	Reference
Australia	1.3	Fitzgerald et al. (1999)
Brazil	1.0	Azevedo (2001)
Canada	MC-LR 1.5	Health Canada (2003)
France	MC-LR 1.0	France (2001)
New Zealand	MC-LR 1.0	Ministry of Health (2005)
USA	EPA	1.6 (age > 6)
		0.3 (age < 6)
	Minnesota	MC-LR 0.1
	Oregon	MC-LR 1.0
		0.3 (age < 6)
	Ohio	1.6 (age 6 ~ adult)
		20 (No contact advisory)
Japan	0.8	
Czech	MC-LR 1.0	Ingrid Chorus, Federal
Denmark	1.0	Environmental Agency
Germany	1.0	(2005)
WHO	MC-LR 1.0	WHO (1998)

Table. 2. The guideline of MCs in recreational water

Country			Guideline (µg/L)
WHO	Relative Probability of Acute Health effects	Low	MC-LR < 10
		Moderate	10-20
		High	20-2,000
		Very high	>2,000
Australia			10
Canada			20
New Zealand			12
USA	Ohio	Public Health Advisory	MC-LR 6
		No Contact Advisory	MC-LR 20
	California		MC-LR 0.8
	IOWA		> 20

<https://www.epa.gov/nutrient-policy-data/guidelines-and-recommendations> (accessed 16 Jun 2016)

Table. 3. Worldwide occurrence of MC-LR in water

Country	Sampling duration	Sampling site (Lake)	Detected concentration (µg/L)	Analytical detection limits (µg/L)	Reference	
USA	Jan ~ Dec (2006)	IOWA			Graham et al. (2010)	
		Beeds	0.39			
		Binder	6.0			
		Clear	1.1			
		Crystal	13			
		East	0.24	0.01		
		Okoboji	0.21			
		Prairie Rose	2,100			
		Rock Creek	0.73			
		Spirit	6.2			
		Upper Gar				
		Kansas				
		Clinton	0.20			
		Miaimi	18	0.01		
		Perry	0.07			
		Prairie	N.D.*			
		Minnesota				
		Albert Lea	1.7			
		Budd	12	0.01		
		Elysian	4.7			
		Loon	1.6			
		Missouri				
		Bilby Ranch	1.7	0.01		
		Mozingo	0.55			

*N.D. (Not detected): below the analytical detection limits.

Table. 3. Worldwide occurrence of MC-LR in water (continued)

Country	Sampling duration	Sampling site (Reservoir)	Detected concentration (µg/L)	Analytical detection limits (µg/L)	Reference
Portugal	Jun (2011)	Alqueva			Rodrigues et al. (2013)
		Ajuda	N.D.*		
		Mourao	0.03	0.01	
		Alamos	0.04		
		Alcarrache	0.05		
	Jul (2011)	Beliche	0.02		
		Alqueva			
		Ajuda	0.29		
		Mourao	0.02	0.01	
		Alamos	0.15		
		Alcarrache	0.12		
		Beliche	0.02		
	Sep (2011)	Alqueva			
		Ajuda	0.34	0.01	
		Mourao	0.22	(**LOQ :	
		Alamos	< LOQ**	0.02)	
		Alcarrache	0.04		
		Beliche	N.D.*		
	Nov (2011)	Alqueva			
		Ajuda	N.D.*	0.01	
		Mourao	0.02	(**LOQ :	
		Alamos	0.02	0.02)	
		Alcarrache	0.43		
		Beliche	< LOQ		

*N.D. (Not detected); below the analytical detection limit; **LOQ (Limit of quantification).

Table. 3. Worldwide occurrence of MC-LR in water (continued)

Country	Sampling duration	Sampling site	Detected concentration (µg/L)	Analytical detection limits (µg/L)	Reference
China	Jan (2014)	Taihu	0.70	-	Xue et al. (2016)
Korea	(2012)	Paldang reservoir	N.D.*	0.05	Ministry of environment (2012-2015)
		Han river, Nakdong river	0.1-51.67		
	(2013)	Nakdong river	N.D.*	0.05	
	(2015)	Han river	< 20	0.05	
	29 Jun (2015)	Seoungsu/Hannam/ Hangang Daegyo	N.D.*	0.05	The office of waterworks Seoul metropolitan government (2016)
		Mapo Daegyo	0.41		
		Seoungsan Daegyo	1.97		
	6 Jul (2015)	Seoungsu/Hannam/ Hangang Daegyo	N.D.*		
		Mapo Daegyo	3.4		
		Seoungsan Daegyo	4.1		

*N.D. (Not detected): below the analytical detection limit.

1.2. Removals and identification of by-products of MC-LR

Once MC-LR is detected in water system, the treatment system operators can act to remove in a number of ways such as conventional treatment (coagulation, sedimentation, filtration), oxidation processes, using membranes, ozonation, and UV processes (US EPA (2012)). To decrease the levels of MC-LR in water, recent studies have examined suitable water treatment technologies, such as conventional water treatment techniques (Chow et al. (1999)), adsorption processes (Huang et al. (2007)), chlorination (Zong et al. (2013); Merel et al. (2009); Zong et al. (2015)), and ozonation (Chang et al. (2014)). Conventional water treatment techniques such as coagulation, sedimentation, and sand filtration would remove algae cells (Keijola et al. (1988)) but sludge containing toxic algae can break down rapidly and release toxic compounds during the process (Huang et al. (2007)). These treatment processes are only efficient for physically removing algae cells, but are not very effective for removing MC-LR in water. Adsorption processes have been shown to be effective in removing MC-LR (Gurbuz et al. (2008)); however, this process needs a relatively high capital cost for treating large amounts of algae. Furthermore, spent adsorbents may be considered hazardous waste. Chlorination has been shown to be effective (Zong et al. (2013), (2015); Merel et al. (2009); Zong et al. (2015)), but the formation of toxic chlorination by-products can be an issue (Zong et al. (2013)). According to Chang et al. (2014), removal is very effective during ozonation. However, formation of disinfection by-products is another potential

problem with the use of ozone when there are high bromide concentrations in the water (US EPA (2012)).

Ultraviolet (UV) treatment is effective in destroying microcystins (US EPA (2012)). However, higher doses than are practicable are required, making it a not viable treatment. Therefore, UV, either alone or in combination with hydrogen peroxide, destroys contaminants in a variety of applications including drinking water, wastewater recycling, and ground water remediation. According to Richard et al. (2014), UV-AOPs have advantages. UV converts hydrogen peroxide into highly reactive hydroxyl radicals which attack and decompose contaminants. At the same time, UV light disinfects the water. For this reasons, MC-LR removal using UV-advanced oxidation processes (AOPs), such as UV photolysis and UV/H₂O₂ (He et al. (2012), (2015)), have been applied. According to previous researches (He et al. (2012), (2015); Chang et al. (2014)), most AOPs efficiently removed MC-LR. There are previous studies using UV-C-AOPs only (He et al. (2012), (2015); Chang et al. (2014)). However, UV-C needs a significant energy for treating MC-LR in water. In addition, typical UV dose for destruction of MC-LR is 1,530-20,000 mJ/cm². Therefore, in terms of energy saving and removal efficiency, UV-B is much efficient than UV-A or UV-C.

Previous studies have focused on removing MC-LR itself. Although the concentration of MC-LR is not detected in water after processes, the major concern with drinking water treatment is the formation of unknown by-products which can

result in secondary pollution. Therefore, it is important to identify by-products and pathways of MC-LR. Previous studies have shown several methods of identification MC-LR by-products during UV-C/AOPs (Zong et al. (2013); He et al. (2015)). Zong et al. (2013) applied UV-C/H₂O₂ for treating MC-LR. They evaluated their generative mechanisms and biological toxicity by mass spectrometry technology and protein phosphatase inhibition assay. They found seven by-products (m/z 783.4, 795.4, 835.4, 1011.1, 1029.6, 1045.5, 1063.5), and proposed pathways. They found major reaction site, which is conjugated diene in ADDA. Toxicity test showed the toxicity of by-products on protein phosphatase 1 decreased, these by-products still possessed certain biological toxicity (especially for m/z 1029.6). He et al. (2015) used UV-C photolysis and UV-AOPs (UV-C/H₂O₂, UV-C/S₂O₈²⁻, and UV-C/HSO₅⁻) for degrading MCs (MC-LR, MC-RR, MC-YR, and MC-LA), and they proposed transformation of MCs in UV-C/H₂O₂ process. They found that the removal of MC-LR by UV/H₂O₂ by UV-254 nm-based processes appeared to be faster than another cyanotoxin. It suggested a faster reaction of MC-LR with hydroxyl radical, which was further supported by the determined second-order rate constant of MCs. They also found mechanisms such as hydroxylation and diene-ADDA double bond cleavage. According to previous researches about UV-AOPs, most of the by-products were higher than m/z 360.

1.3. Objectives

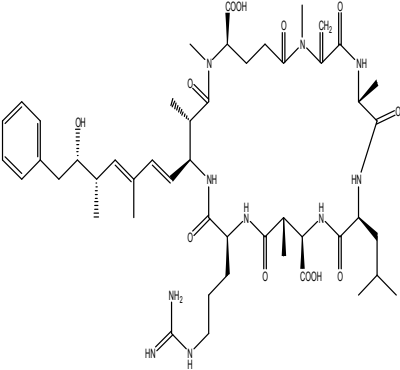
The objectives of this study were: (1) to compare the removal of MC-LR by UV-B photolysis and UV-B/H₂O₂ processes; (2) to determine the kinetics during two processes; (3) to identify degradation by-products produced during each process using liquid chromatography-tandem mass spectrometry (LC-MS/MS) and ACD/MS Fragmenter software; (4) to propose possible degradation pathways and potential degradation mechanisms of two processes.

2. Materials and Methods

2.1. Chemicals

MC-LR was purchased from Alexis-Enzo Life Sciences (Farmingdale, NY). Table 4 shows the physicochemical properties of MC-LR. The stock solution of 1000 mg/L was prepared by adding 1 mg MC-LR in 1 mL LC/MS grade methanol (Fisher Scientific, Pittsburgh, PA, USA) (Merel et al. (2009); Jing et al. (2014)), then was diluted in distilled water obtained from a Millipore Milli-Q system. MC-LR solution was stored in darkness at -20°C. Hydrogen peroxide (30%, v/v) and formic acid (88%, v/v) were purchased from Sigma-Aldrich.

Table. 4. Physicochemical properties of MC-LR

Molecular structure	Properties
	Molecular formula: C ₄₉ H ₇₄ N ₁₀ O ₁₂
	Exact mass: 995.17
	Density: 1.299 g/cm ³
	Solubility in ethanol: 1 mg/mL
	Log P (Partition coefficient): -1.44
	LD ₅₀ : 5 mg/kg (Mouse, Oral)

2.2. Experimental procedures

For the removal of MC-LR, UV photolysis and UV/H₂O₂ processes were conducted using a batch type reactor (Figure. 1(a)). UV chamber consists of three UV-B lamps (6 W, 312 nm, San-Kyo Electrics, Japan). UV intensity was measured with a radiometer (VLX-3W Radiometer 9811-50, Cole-Parmer, USA). The intensity values of UV light were 0.47, 0.58, and 1.57 mW/cm² (applied UV fluence: 1,692, 2,088, and 5,652 mJ/cm²), respectively. The initial MC-LR concentration was 100 µg/L and H₂O₂ dose of 1, 2, and 4 mg/L were used. Sampling time was 0, 10, 20, 30, 60, 90, and 120 min, respectively.

For the identification by-products of MC-LR, the initial MC-LR concentration was 100 µg/L and H₂O₂ dose of 1 mg/L were used. According to Table 3, Detected concentration of MC-LR is lower than 100 µg/L. However, when a bloom occurs, detected concentration was higher than general detected concentration. In addition, in order to get more detail information related by-products, the initial MC-LR concentration was determined. Solution containing MC-LR (100 µg/L) was stirred to maintain homogeneous solution. UV photolysis and UV/H₂O₂ reactions were conducted using a photo-reactor (Figure. 1(b)). Photo-reactor system consists of a 2 L glass bottle with side arms, a peristaltic pump for circulating solution, six quartz columns, and UV chamber. Six quartz columns consist of flexible Teflon tubing. Typical UV dose for destruction of MC-LR is 1,530 ~ 20,000 mJ/cm² (Croll and Hart (1996)). In order to totally remove MC-LR, UV chamber consists of six UV-B

lamps and the intensity values of UV light were 5.74 mW/cm^2 (applied UV fluence: $20,664 \text{ mJ/cm}^2$) and 5.68 mW/cm^2 (applied UV fluence: $20,448 \text{ mJ/cm}^2$) during UV-B photolysis and UV-B/ H_2O_2 processes, respectively.

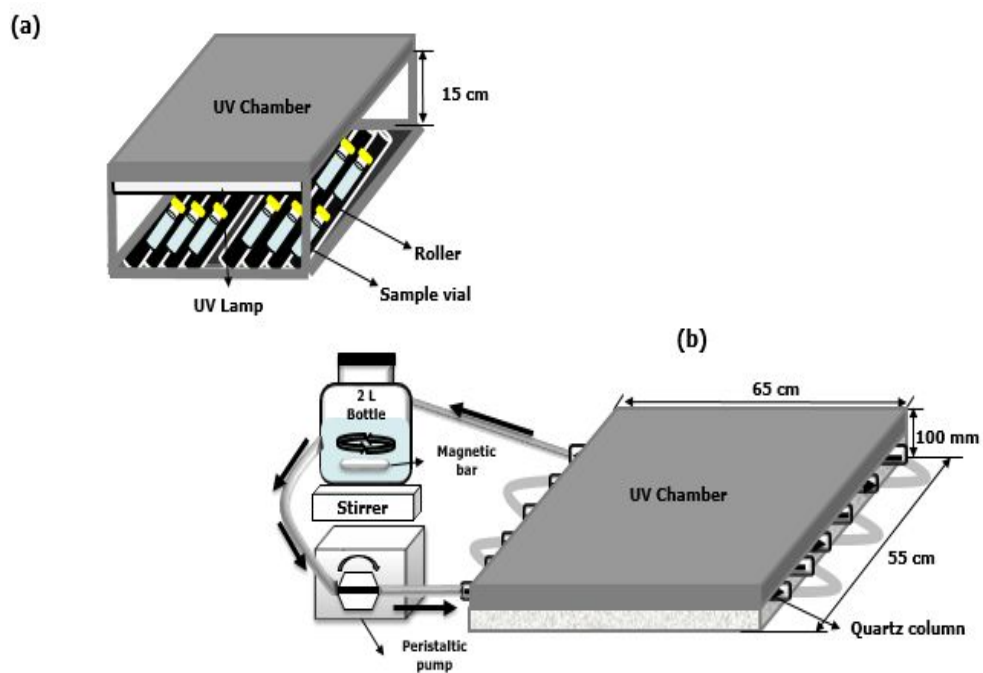


Figure. 1. Schematic diagram of a photolytic reactor.

2.3. Analytical methods

Before analysis, 50 mL of samples were pre-treated with SPE (solid-phase extraction). SPE was conducted using a HLB (hydrophile-lipophile balance) cartridge (Oasis HLB, Waters, Milford, MA, USA). The HLB cartridges were conditioned with 5 mL methanol and water. After loading the samples, the cartridges were dried for 10 min and then eluted with 6 mL of formic acid (0.1 %, v/v) in methanol. 6 mL of eluting solution was concentrated using centrifugal concentrator (CVE-3100, EYELA, Japan) during 24 hr. Then, 1 mL of methanol was added to the collected sample. Finally, the final sample volume was reconstituted to 1 mL (Qiao et al. (2005)). The concentration of MC-LR was determined by UPLC (Ultra-performance liquid chromatograph) (Nexera, Shimadzu, Japan) equipped with API-4000 mass spectrometer (AB SCIEX, USA). The column was C₁₈ column (2.1 x 100 mm, 3.5 µm, XBridge, USA). Mobile phase A was formic acid (0.1 %, v/v) in water and B was methanol only (Jing et al., 2014). Mobile phase condition was isocratic mode (A/B=2/98) and ionization mode was used positive mode. Also, the flow rate was 0.2 mL/min and the injection volume was 20 µL. Optimized LC-MS/MS condition of MC-LR is shown in Table 5 and Figure 2 is shown LC-MS/MS chromatogram of MC-LR. Range of calibration curve was 1, 2, 5, 10, 20, 50, and 100 µg/L. Method detection limit (MDL) in distilled water samples was estimated with seven replicates using 1 µg/L of MC-LR standard solution. Method detection limit (MDL) and Limit of quantification (LOQ)

were 0.13 µg/L and 0.40 µg/L, respectively.

For the identification of by-products during reactions, after extraction, 5 mL of samples were full scanned by API-4000 mass spectrometer (AB SCIEX, USA). Mass spectra were obtained by direct injection into mass spectrometer using a Harvard syringe pump (Model 975 Harvard Apparatus, Dover, MA, USA). Fragmentation of the precursor ion was conducted to confirm their product ions using collision energy with nitrogen gas. For eliminating the matrix m/z values, distilled water and methanol solvent were analyzed using MS analysis by full scanning from m/z 50 to 250, 250 to 500, 500 to 750, and 750 to 1200, respectively. Then, to obtain the fragmentation data of degradation by-products, the positive ion mode was used by full scanning from m/z 50 to 250, 250 to 500, 500 to 750, and 750 to 1200, respectively. By-products were identified peak areas using LC-MS/MS. The possible chemical structures and degradation pathways of by-products were proposed according to the results of using ACD/MS Fragmenter (ACD Labs, Advanced Chemistry Development, Inc., Canada).

Table. 5. Optimized LC-MS/MS condition for the analysis of MC-LR

Compounds	Parent ion (m/z)	Product ion (m/z)	Time (msec)	Collision energy (mV)	Collision cell exit potential (mV)
MC-LR	995.6	135.3	40.5	95	16
		213.3	40.5	93	22

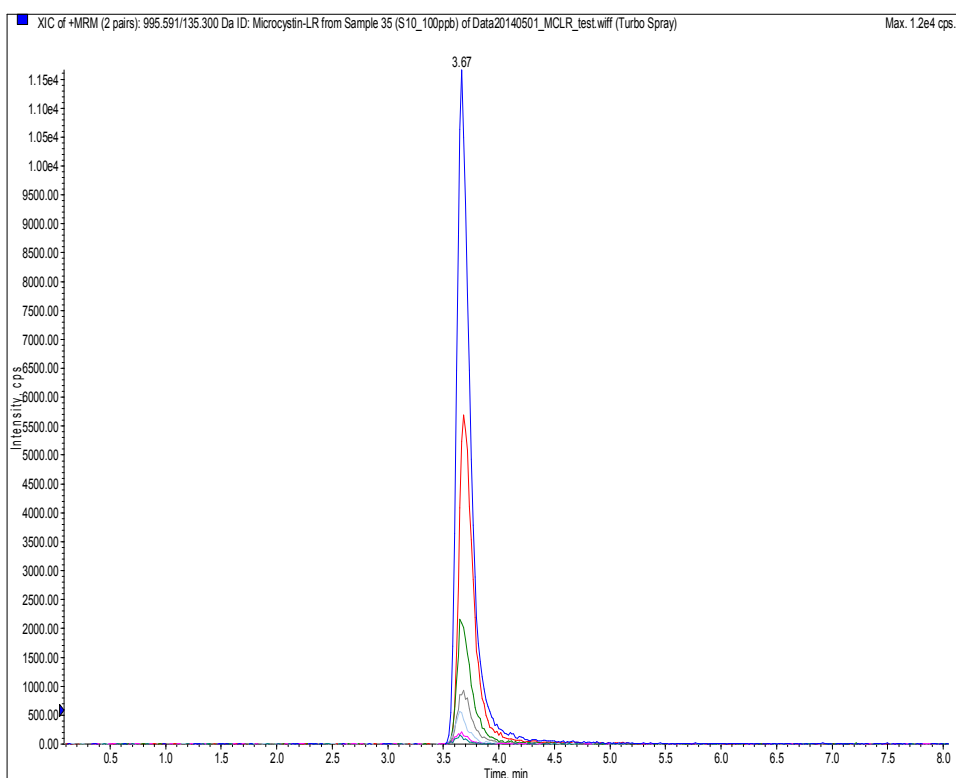


Figure. 2. LC-MS/MS chromatograms of MC-LR (retention time: 3.67 min; $r^2=0.9997$).

3. Results and discussion

3.1 Kinetics

Figure 3 shows the removal of MC-LR during UV-B photolysis and UV-B/H₂O₂ processes. Compared to UV-B photolysis, the UV-B/H₂O₂ process more effectively removed MC-LR. Table 6 summarizes the rate constants (k) and R² during the two processes. According to He et al. (2015), second-order reaction during UV-C/H₂O₂ processes. However, in this study, both the UV-B photolysis and UV-B/H₂O₂ processes the second-order kinetics can be well approximated as first order kinetics which is pseudo first-order reactions (Table 6). If the concentration of one relative reactant remains constant because it is supplied in great excess ([B]>>[A]), obtaining the pseudo first order reaction constant (Eq. (1)).

$$r = k[A][B] = k'[A] \text{ (r: rate A, B: reactants; k, k'=rate constant) } \quad (1)$$

The OH radical can be effectively produced by combining the reaction of UV with H₂O₂. Not only does a photolysis occur, but the OH radical can also be effectively produced by UV-B/H₂O₂ process ((Eq. (2)~(4)). The major mechanism during the UV-B/H₂O₂ process is the cleavage of the molecule by OH radicals (Legrini et al. (1993)).

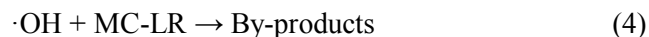
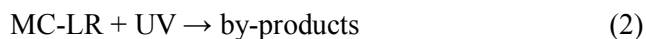


Figure 4 shows the effects of UV-B intensity and H₂O₂ dose. Data was obtained for three different UV-B intensities using different UV-B lamps (0.47, 0.58, and 1.57 mW/cm²) and three different concentrations of H₂O₂ (1, 2, and 4 mg/L). The removal of MC-LR increased as the UV-B intensity increased (Figure 4(a)). UV dose needed for destruction of MC-LR is 1,530 ~ 20,000 mJ/cm² (Croll and Hart (1996)). In this study, UV-B photolysis (applied UV fluence: 1,692 ~ 5,652 mJ/cm²) removed more than 40 % of MC-LR compounds within an hour, and followed pseudo first-order kinetics. The removal of MC-LR also increased as the H₂O₂ dose increased (Figure 4(b)). All reactions were pseudo first-order reactions (Table 6). The optimization of MC-LR removal and the UV-B intensity and H₂O₂ dose are required when applying the UV-B/H₂O₂ process in water treatment plants (WTPs).

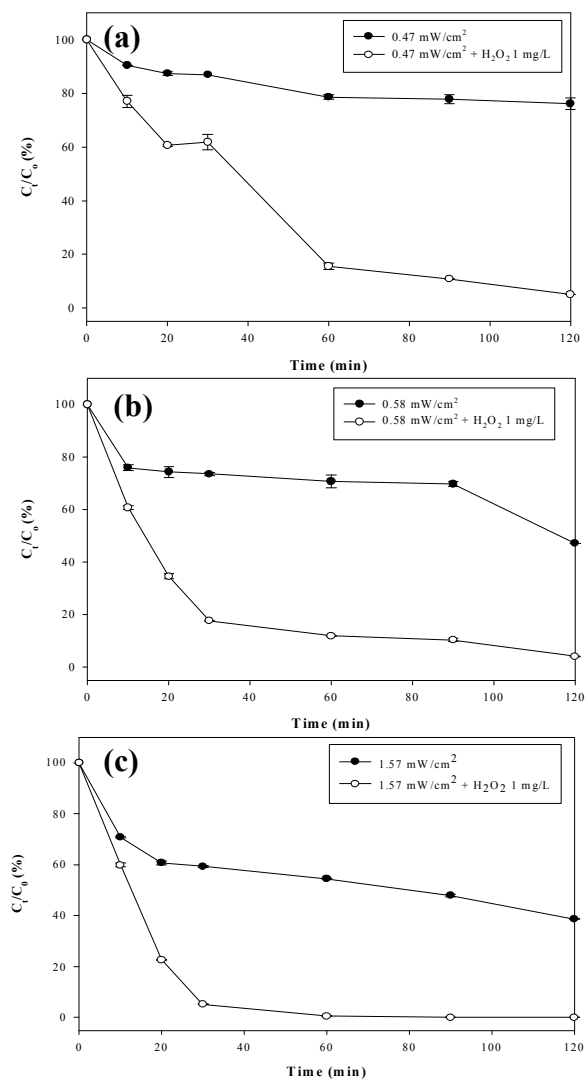


Figure. 3. Removal of microcystin-LR (MC-LR) during the UV-B photolysis and UV-B/H₂O₂ processes at different UV intensities: (a) 0.47, (b) 0.58, and (c) 1.57 mW/cm² (n = 2, [C₀] = 100 µg/L, [H₂O₂] = 1 mg/L, 20°C).

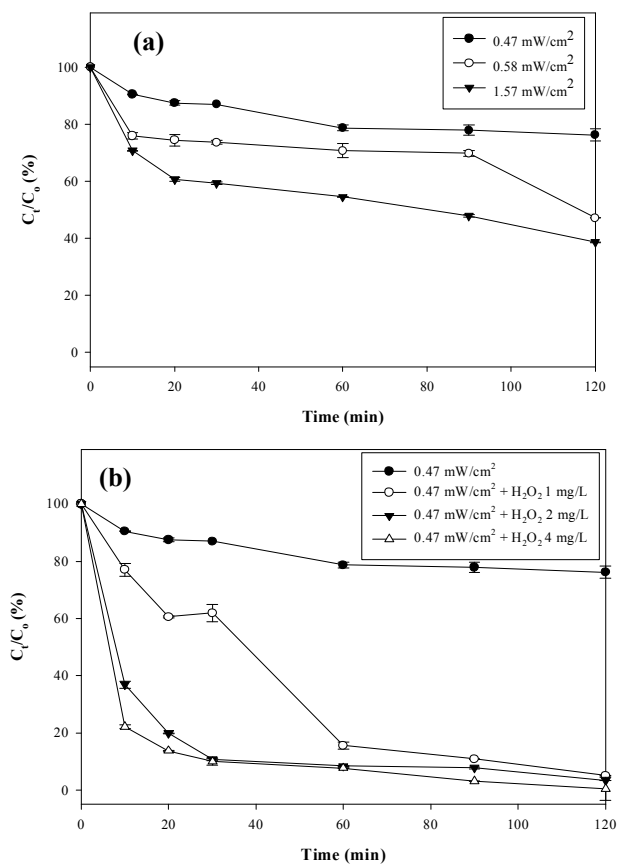


Figure. 4. Effect of UV intensity (a) and H₂O₂ dose (b) ($n = 2$, $[C_0] = 100 \mu\text{g/L}$, UV intensity = 0.47, 0.58, and 1.57 mW/cm², $[\text{H}_2\text{O}_2] = 1, 2, \text{ and } 4 \text{ mg/L}$, 20°C).

Table. 6. Changes in rate constants (k) and R² by adjusting the UV intensity and H₂O₂ dose during the UV-B photolysis and UV-B/H₂O₂ processes

Condition	k (min ⁻¹)	R ²
0.47 mW/cm ²	0.0020	0.8338
0.47 mW/cm ² + H ₂ O ₂ 1 mg/L	0.0227	0.8021
0.47 mW/cm ² + H ₂ O ₂ 2 mg/L	0.0255	0.9750
0.47 mW/cm ² + H ₂ O ₂ 4 mg/L	0.0350	0.8977
0.58 mW/cm ²	0.0043	0.7487
0.58 mW/cm ² + H ₂ O ₂ 1 mg/L	0.0234	0.8962
1.57 mW/cm ²	0.0061	0.8312
1.57 mW/cm ² + H ₂ O ₂ 1 mg/L	0.0758	0.9876

3.2 Identification of the by-products of MC-LR

The degradation by-products of MC-LR were identified during UV-B photolysis and UV-B/H₂O₂ processes. The product ions of the degradation by-products with the highest peak intensity (more than 5.5×10^5) or peak area were selected using a mass spectrometer. Table 6 shows the fragmentation results obtained by LC-MS/MS for the MC-LR degradation by-products during the UV-B photolysis and UV-B/H₂O₂ processes.

During UV-B photolysis, eight by-products were identified from the degradation of MC-LR, with m/z 414.3, 417.3, 709.6, 428.9, 608.6, 847.5, 807.4, and 823.6. In contrast, eleven major by-products were confirmed following the degradation of MC-LR during the UV-B/H₂O₂ process, with m/z 707.4, 414.7, 429.3, 445.3, 608.6, 1052.0, 313.4, 823.6, 357.3, 245.2, and 805.7 (Table 7). The identified by-products during the two processes are numbered in order of the occurrence of maximum points.

During the two processes, most MC-LR degradation by-products (except for the m/z 1052.0 in the UV-B/H₂O₂ process) had lower m/z values than the precursor ion of MC-LR (m/z 995.6), indicating that the major reaction was a cleavage or breakdown reaction. According to recent studies of the UV-based AOPs, no by-products of MC-LR with an m/z value less than m/z 360 have been identified by LC-MS/MS (Kaya et al. (1998); Antoniou et al. (2008); Merel et al. (2009); Chang

et al. (2014); He et al. (2015)). However, in this study, new by-products with an m/z value less than m/z 360 (m/z 245.2, 313.4, and 357.3) were identified as by-products during the UV-B/H₂O₂ process. Interestingly, two by-products with m/z 608.6 and 823.6 were produced during both the UV-B photolysis and UV-B/H₂O₂ processes.

Table. 7. Fragmentation results for MC-LR degradation by-products during the UV-B photolysis and UV-B/H₂O₂ processes

UV-B photolysis						
Compound	Chemical Formula	Monoisotopic Mass (Da)	Precursor ion (m/z)	Product ions (m/z)		
MC-LR	C ₄₉ H ₇₄ N ₁₀ O ₁₂	994.5	995.6	135.3	213.3	
By-product 1	C ₂₃ H ₃₀ N ₂ O ₅	414.2	414.3	171.1	189.0	301.1
By-product 2	C ₂₃ H ₃₂ N ₂ O ₅	416.2	417.3	303.2		
By-product 3	C ₃₁ H ₅₂ N ₁₀ O ₉	708.4	709.6	317.1		
By-product 4	C ₁₇ H ₂₉ N ₇ O ₆	427.2	428.9	39.2		
By-product 5	C ₂₉ H ₄₉ N ₇ O ₇	607.4	608.6	57.3	71.3	
By-product 6	C ₃₉ H ₆₂ N ₁₀ O ₁₁	846.5	847.5	445.2	446.3	641.4
By-product 7	C ₃₆ H ₅₈ N ₁₀ O ₁₁	806.4	807.4	415.2	416.3	417.3
By-product 8	C ₄₀ H ₅₇ N ₉ O ₁₀	823.4	823.6	429.2	430.1	39.2
UV-B/H ₂ O ₂ process						
Compound	Chemical Formula	Monoisotopic Mass (Da)	Precursor ion (m/z)	Product ions (m/z)		
MC-LR	C ₄₉ H ₇₄ N ₁₀ O ₁₂	994.5	995.6	135.3	213.3	
By-product 1	C ₃₁ H ₅₀ N ₁₀ O ₉	706.4	707.4	317.0	318.2	205.1
By-product 2	C ₂₄ H ₃₈ N ₄ O ₂	414.3	414.7	303.1	302.6	189.0
By-product 3	C ₂₄ H ₃₆ N ₄ O ₃	428.3	429.3	302.3	301.2	
By-product 4	C ₂₄ H ₃₆ N ₄ O ₄	444.3	445.3	123.3		
By-product 5	C ₂₉ H ₄₉ N ₇ O ₇	607.4	608.6	57.3	71.3	317.1
By-product 6	C ₃₆ H ₅₆ N ₁₀ O ₁₁	804.4	805.7	414.2	415.3	415.9
By-product 7	C ₂₀ H ₂₇ NO ₂	313.2	313.4	128.1	93.2	
By-product 8	C ₄₀ H ₅₇ N ₉ O ₁₀	823.4	823.6	430.1	39.2	
By-product 9	C ₂₂ H ₃₂ N ₂ O ₂	356.2	357.3	98.8		
By-product 10	C ₁₇ H ₂₄ O	244.2	245.2	44.3		
By-product 11	C ₅₆ H ₇₇ N ₉ O ₁₁	1051.6	1052.0	414.3	660.2	

3.3 Time profiles of the degradation by-products of MC-LR

The degradation by-products of MC-LR were identified and confirmed using mass spectrometry and LC-MS/MS (Table 7). The peak areas of degradation by-products during two processes were measured using the fragmentation results (Table 7) and LC-MS/MS fragmentation data (Table 8-9). The time profiles of the degradation by-product peak areas during the UV-B photolysis and UV-B/H₂O₂ processes are shown in Figures 5 and 6, respectively. The identified by-products during the two processes are numbered in order of the occurrence of maximum points (Table 7).

During the UV-B photolysis, by-product 1 (m/z 414.3) was a major by-product and had an maximum point (Figure 5(a)). Due to the different scale for the peak areas of the by-product, the time profiles were separately provided. Figure 5(b) also shows the maximum points in the order of by-product 2 (m/z 417.3), by-product 3 (m/z 709.6), and by-product 4 (m/z 428.9). Similarly, Figure 5(c) shows the maximum point in the order of by-product 6 (m/z 847.5), and by-product 7 (m/z 807.4). However, the peak area of by-product 8 (m/z 823.6) continued to rise as the reaction proceeded.

The time profiles of degradation by-products during the UV-B/H₂O₂ process are summarized in Figure 6. Among the identified by-products, by-product 1 (m/z 707.4), by-product 2 (m/z 414.7), and by-product 3 (m/z 429.3) had the largest peak

areas (Figure. 5(a)). Due to the different scale of the areas of by-product peaks, the time profiles of the by-products, except by-products 1, 2, and 3, are provided separately in Figure 6(b). Figure 6(b) shows maximum points in by-product 4 (m/z 445.3), by-product 6 (m/z 805.7), by-product 7 (m/z 313.4), and by-product 8 (m/z 823.6). Interestingly, by-product 5 (m/z 608.6) and by-product 8 (m/z value of 823.6) were produced during both the UV-B photolysis and UV-B/H₂O₂ processes. The peak area of by-product 11 (m/z value of 1052.0) continued to rise as the reaction progressed (Figure 6(b)).

The peak areas of most degradation by-products decreased during the UV-B/H₂O₂ process, except by-products 6, 10, and 11, for which the m/z values corresponded to 805.7, 245.2, and 1052.0, respectively (Figure 7 and Table 7). According to the molecular structure identified by the ACD software, by-product 10 (m/z 245.2) and by-product 6 (m/z 805.7) corresponded to ADDA and main ring which is removing a ADDA from the cyclic heptapeptide, respectively. While MC-LR has a three-dimensional structure, the cyclic heptapeptide (by-product 6) is planar, and ADDA (by-product 10) has a U-shape (Lanaras et al. (1991)). The fact that the peak area of these by-products (by-products 6 and 10) continued to increase as the reaction progressed can be explained by the planar type structures. The peak area of by-product 11 also continued to increase as the reaction progressed (Figure 7). By-product 11 (m/z 1052.0) had a higher m/z value than the precursor ion of MC-LR (m/z 995.6), indicating that it should be occurred adduct reaction. Its m/z

value is corresponded with an adduct product between the by-products.

Table. 8. Optimized LC-MS/MS conditions for the analysis of MC-LR and its by-products during UV-B photolysis

Compounds	Parent ion (m/z)	Product ion (m/z)	Time (msec)	Collision energy (mV)	Collision cell exit potential (mV)
MC-LR	995.6	135.3, 213.3	40.5	95, 93	16, 22
By-product 1	414.3	171.1, 189.0, 301.1	40.5	29, 29, 27	10, 20, 18
By-product 2	417.3	303.2	40.5	27	20
By-product 3	709.6	317.1	40.5	43	22
By-product 4	428.9	39.2	40.5	43	4
By-product 5	608.6	57.3, 71.3	40.5	61, 53	6, 8
By-product 6	847.5	445.2, 446.3, 641.4	40.5	17, 13, 13	22, 30, 16
By-product 7	807.4	415.2, 416.3, 417.3	40.5	23, 23, 21	18, 20, 20
By-product 8	823.6	429.2, 430.1, 39.2	40.5	17, 15, 17	26, 26, 22

Table. 9. Optimized LC-MS/MS conditions for the analysis of MC-LR and its by-products during UV-B/H₂O₂ process

Compounds	Parent ion (m/z)	Product ion (m/z)	Time (msec)	Collision energy (mV)	Collision cell exit potential (mV)
MC-LR	995.6	135.3, 213.3	40.5	95, 93	16, 22
By-product 1	707.4	317.0, 318.2, 205.1	40.5	45, 45, 59	20, 12, 18
By-product 2	414.7	303.1, 302.6, 189.0	40.5	25, 27, 29	12, 12, 20
By-product 3	429.3	302.3, 301.2	40.5	27, 29, 53	12, 20, 14
By-product 4	445.3	123.3	40.5	35	12
By-product 5	608.6	57.3, 71.3, 317.1	40.5	59, 49, 47	20, 14, 12
By-product 6	805.7	414.2, 415.3, 415.9	40.5	23, 23, 23	8, 8, 20
By-product 7	313.4	128.1, 93.2	40.5	27, 49	12, 10
By-product 8	823.6	430.1, 39.2	40.5	17, 63	20, 8
By-product 9	357.3	98.8	40.5	39	12
By-product 10	245.2	44.3	40.5	49	8
By-product 11	1052.0	414.3, 660.2	40.5	32,37	20, 18

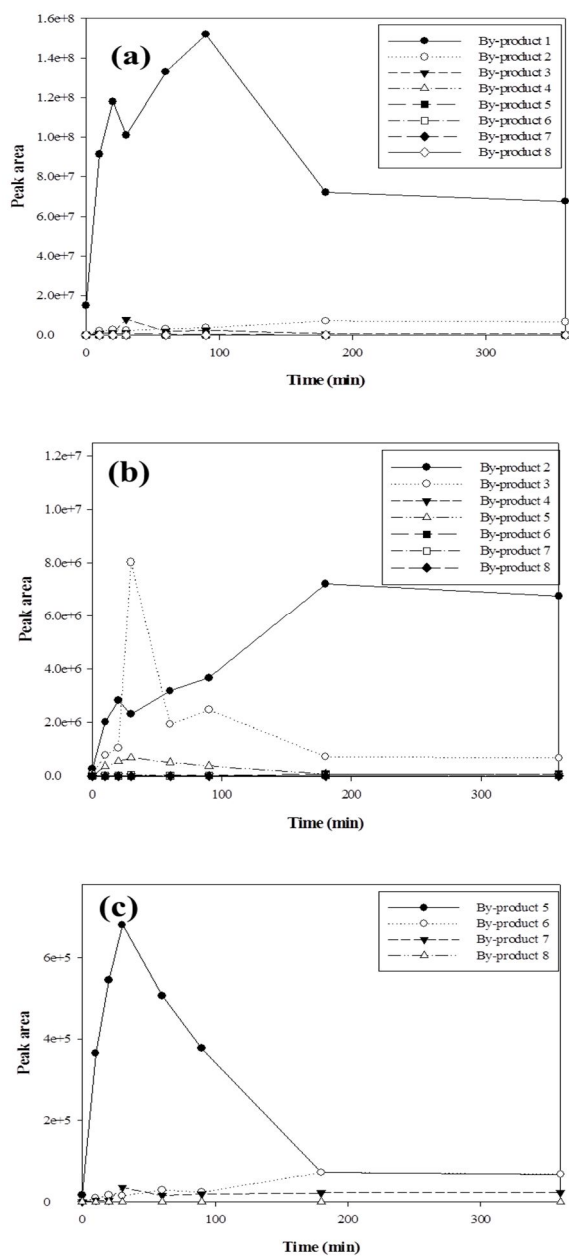


Figure. 5. Time profiles of the degradation by-products during UV-B photolysis ($[C_0] = 100 \mu\text{g/L}$, UV intensity = 5.74 mW/cm^2 , 20°C , reaction time = 6 h).

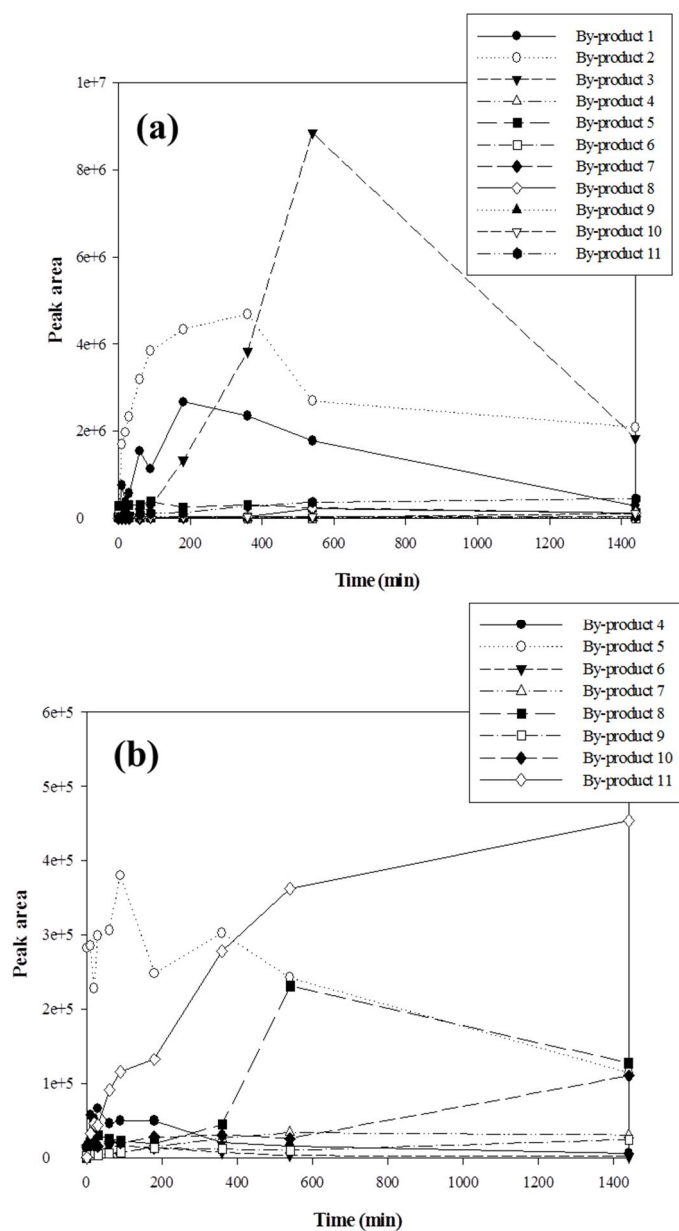


Figure. 6. Time profiles of the degradation by-products by UV-B/H₂O₂ process ($[C_0] = 100 \mu\text{g/L}$, $[\text{H}_2\text{O}_2] = 1 \text{ mg/L}$, UV intensity = 5.68 mW/cm^2 , 20°C , reaction time = 24 h).

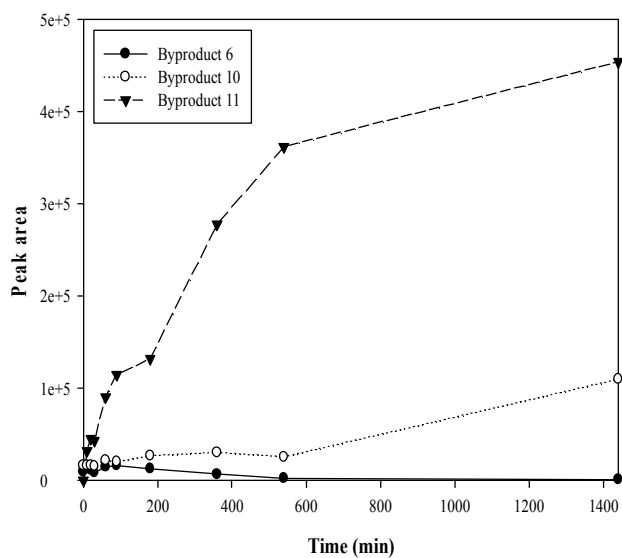


Figure. 7. Time profiles of each by-product by UV-B/H₂O₂ process ([C₀] = 100 µg/L, [H₂O₂] = 1 mg/L, UV intensity = 5.68 mW/cm², 20°C, reaction time = 24 h).

3.4 Degradation mechanisms and pathways of the identified by-products

Using the identified by-products, the maximum points of the by-product peak areas, ACD/MS Fragmenter software, and molecular weights, possible structures of the by-products were determined. The mechanisms and pathways of the UV-B photolysis and UV-B/H₂O₂ processes were proposed as follows.

During UV-B photolysis, there are two main mechanisms that produce by-products: bond cleavage of C-C or C-N single bonds and nitrogen free electron pair transfer. With regard to the first mechanism, MC-LR (m/z 995.6) has a bulky structure that contains a main ring which is removing a ADDA from the cyclic heptapeptide. According to previous studies (Zong et al. (2013; He et al. (2015))), the major reaction site is conjugated diene in ADDA. However, in this study, there are bond cleavage reactions of the C-C or C-N single bond. MC-LR has a three-dimensional structure; the cyclic heptapeptide is planar, ADDA is U-shaped, and an angle of 90° is formed when the cyclic heptapeptide fits through the ADDA (Lanaras et al. (1991)). For this reason, during both processes, the major degradation reaction sites are the main ring on the left of the MC-LR molecule, which is in contiguity with the ADDA. Therefore, the major degradation reactions during UV-B photolysis are the main ring-opening of the MC-LR molecule, which is referred to as bond cleavage of the C-C or C-N single bond.

With regard to the second mechanism, MC-LR has 10 nitrogen atoms that have a free electron pair. During UV-B photolysis, the free electron pair of the nitrogen atom in MC-LR can be excited from the stable state, resulting in free electron pair transfer during processes. Due to the free electron pair transfer reaction containing nitrogen atoms (Rajaratnam et al. (1992)), intramolecular rearrangement of free electrons in the nitrogen atoms (Ulstrup et al. (1975)) in the MC-LR structure is possible during the UV-B photolysis.

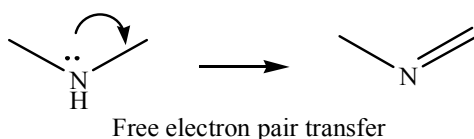


Figure 8 summarizes the proposed degradation pathways of by-products during UV-B photolysis. As shown in Figure 8, there are two main mechanisms (bond cleavage and a nitrogen free electron pair transfer reaction) that occur during UV-B photolysis. First, by-product 2 (m/z 417.3) is formed by the bond cleavage of a C_{13} - C_{14} and C_{31} - C_{32} single bond in the MC-LR molecule. By-product 1 (m/z 414.3) can be formed by a free electron pair transfer reaction at the nitrogen atom of by-product 2 (the N_{33} electron pair is transferred to C_9 , resulting in the formation of the $N_{33}=C_9$ double bond in by-product 1). Next, by-product 3 (m/z 709.6) is formed by bond cleavage of the C_8 - C_9 , N_{12} - C_{13} and C_{14} - C_{15} single bonds, respectively. This by-

product 3 can be an intermediate of by-product 4 (m/z 428.9). By-product 6 (m/z 847.5) can be formed by the bond cleavage of the C_4-C_5 bond in ADDA in the MC-LR molecule. Which is reported degradation mechanism of MC-LR including diene-ADDA double bond cleavage by-products (He et al. (2015)), but, possible structure of by-product is different. By-product 4 can be formed by the bond cleavage of the $C_{24}-C_{25}$ single bond at by-product 6. By-product 7 can be formed by the bond cleavage of the C_6-C_7 single bond at by-product 6. Finally, by-product 5 (m/z 608.6) can be formed by the bond cleavage of the C_4-C_5 , $C_{11}-N_{12}$, and $N_{20}-C_{21}$ single bonds of MC-LR. By-product 8 is formed by the bond cleavage of the C_3-C_4 , $C_{31}-C_{32}$, and C_9-N_{33} single bonds of the MC-LR molecule, followed by a free electron pair transfer reaction at the nitrogen atoms (N_{20} , N_{23} , N_{26} , N_{30} , and $N_{3'}$). Thus, by-product 8 has five $N=C$ double bonds.

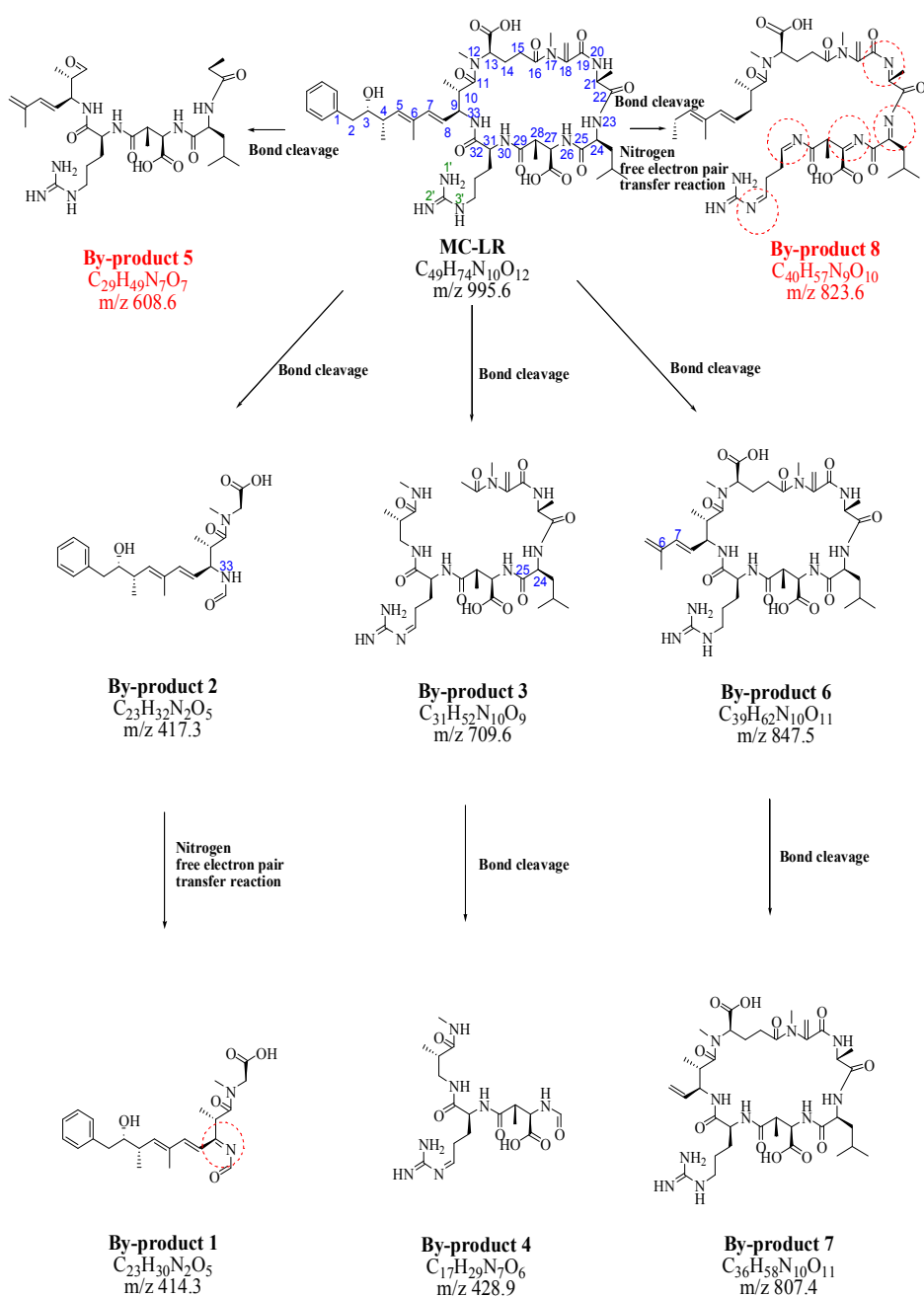


Figure. 8. Proposed MC-LR degradation pathways for UV-B photolysis.

During the UV-B/H₂O₂ process, along with bond cleavage and nitrogen free electron pair transfer reactions, a reaction with the OH radical and an adduct reaction were found to occur (Figure 9). The previous studies reported the mechanisms for OH radical attack at the aromatic ring, methoxy group, and conjugated double bond of the ADDA during the degradation reaction (Antoniou et al. (2008); He et al. (2015)). In this study, the conjugated diene of the ADDA and carbon site was also found to be a major target site for OH radical attack during the UV/H₂O₂ process. Unlike previous studies, in this study, adduct reaction were found to occur.

Details of the proposed mechanisms during the UV/H₂O₂ process are shown in Figure. 8. Interestingly, by-product 5 (m/z 608.6) and by-product 8 (m/z 823.6) were produced during both the UV-B photolysis and UV-B/H₂O₂ processes.

By-product 1 (m/z 707.4) was formed by two mechanisms. First, bond cleavage of the N₁₂-C₁₃ and C₁₄-C₁₅ single bonds, and C₇=C₈ double bond, followed by a free electron pair transfer reaction at N₁₂ and N₃. By-product 4 (m/z 445.3) can be formed by three steps. First, by-product 2 (m/z 414.7) is formed by bond cleavage of the C₁₀-C₁₁ and N₃₀-C₃₁ single bonds in the MC-LR molecule. Then, by-product 3 (m/z 429.3) is formed by an N₃₃ and N₃ free electron pair transfer reaction and the addition of an OH radical at C₇.

The conjugated carbon double bonds in the ADDA can cause PP1 and PP2A (phosphatase type 1 and type 2A) inhibition, indicating that this site may be

responsible for MC-LR toxicity (Dawson et al. (1998); Gullledge et al. (2002)). For this reason, the formation of by-product 3 (m/z 429.3) might eliminate the toxicity of MC-LR itself. Finally, by-product 4 (m/z 445.3) was formed by the addition of the OH radical at C₃₁. By-product 7 (m/z 313.4) can be formed by bond cleavage of the N₁₂-C₁₃ and C₉-N₃₃ single bonds and an N₁₂ electron pair transfer reaction of the MC-LR molecule.

For the formation of by-product 10 (m/z 245.2), by-product 7 (m/z 313.4) can be the intermediate. By-product 10 (m/z 245.2) can be formed by bond cleavage of the C₁₀-C₁₁ single bond of by-product 7, followed by elimination of the methyl group. By-product 9 (m/z 357.3) can be produced by bond cleavage of the C₁₄-C₁₅, C₃₂-N₃₃, and C₁₅-C₁₆ single bonds, and an N₃₃ free electron pair transfer reaction from MC-LR. By-product 6 (m/z 805.7) is formed by bond cleavage of the C₆-C₇ bond of the MC-LR molecule. Interestingly, during the UV/H₂O₂ process, by-product 11 (m/z 1052.0) was found, the molecular weight of which is higher than that of the precursor ion of MC-LR (m/z 995.6); therefore, it was predicted as an adduct product between by-product 6 and by-product 10.

Finally, Figure 10 shows changes in the sum of the peak area for by-products identified during the UV-B/H₂O₂ process at different H₂O₂ concentrations. While the accumulated peak areas of by-products identified with 1 mg/L H₂O₂ kept increasing, the accumulated peak areas were much lower and decreased after 30 min with 4 mg/L H₂O₂. The peak areas of MC-LR degradation by-products decreased as

the H_2O_2 dose increased, indicating that the peak areas of the by-products decreased as the reaction progressed. Based on these data, the degradation by-products identified here can be effectively eliminated by further increasing the H_2O_2 dose during the UV/ H_2O_2 process.

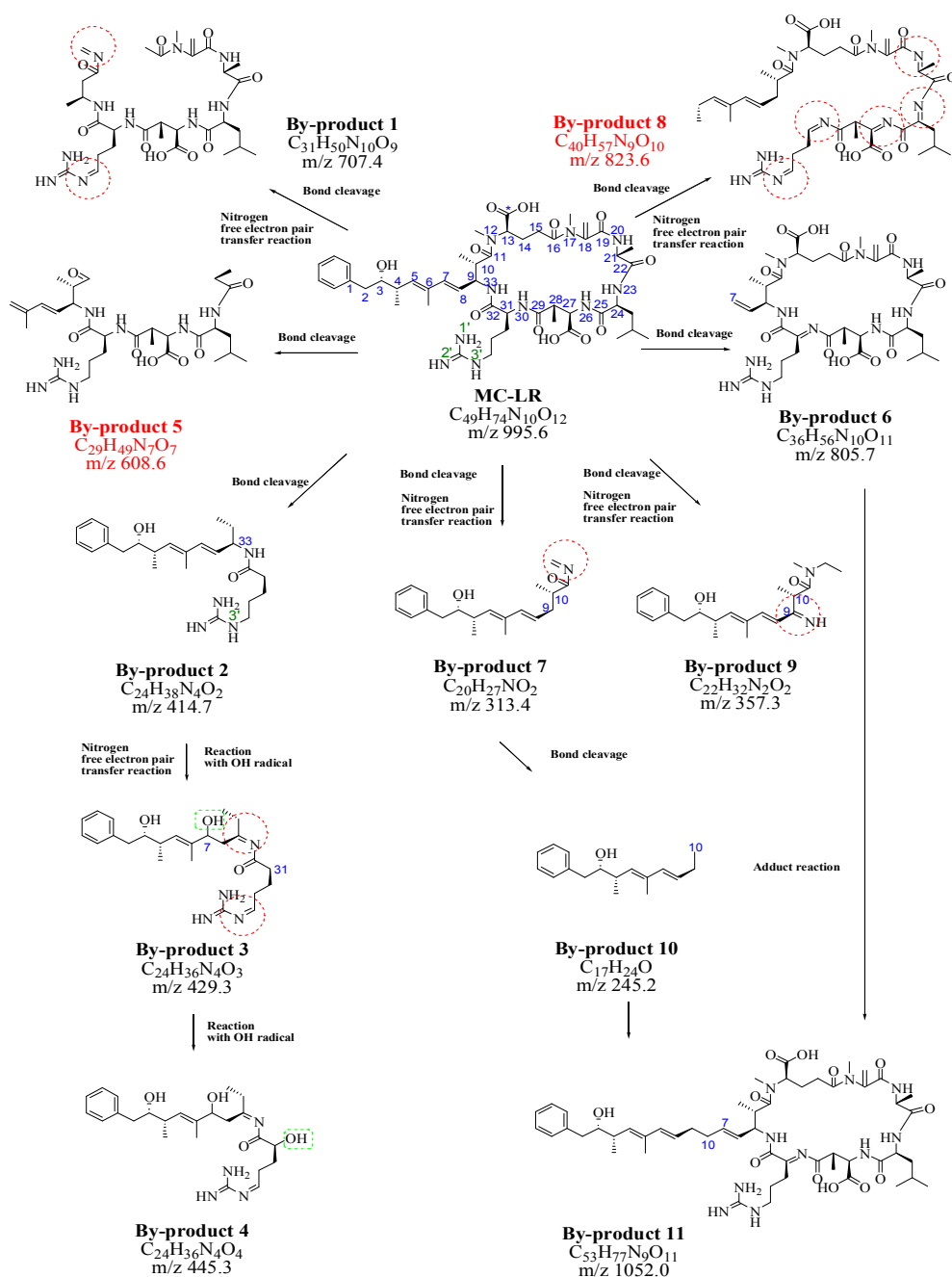


Figure. 9. Proposed MC-LR degradation pathways for the UV-B/ H_2O_2 process.

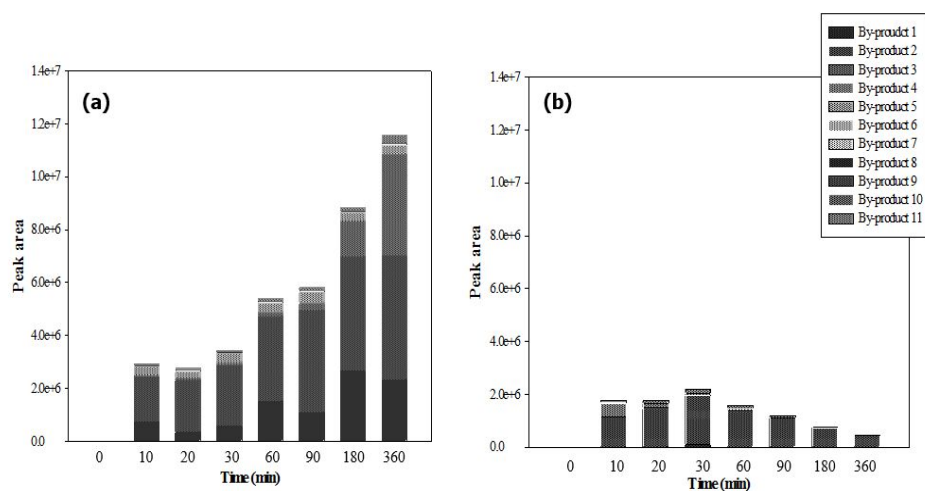


Figure. 10. Changes in accumulated peak area for the identified by-products during the UV-B/ H_2O_2 process with a H_2O_2 dose of (a) 1 mg/L or (b) 4 mg/L ($[\text{C}_0] = 100 \mu\text{g/L}$, UV intensity = 5.68 mW/cm^2 , 20°C , reaction time = 6 h).

4. Conclusions

In this study, the removal and degradation mechanisms of MC-LR during UV-B photolysis and UV-B/H₂O₂ processes were investigated. The intensity values of UV light were 0.47, 0.58, and 1.57 mW/cm² (applied UV fluence: 1,692, 2,088, and 5,652 mJ/cm²), respectively. The kinetics results showed that the UV-B/H₂O₂ process more effectively removed MC-LR than UV-B photolysis. The removal of MC-LR increased as the UV intensity and H₂O₂ dose increased. All degradation reactions followed pseudo first-order reactions.

For the identification by-products of MC-LR, in order to totally remove MC-LR, the intensity values of UV light were 5.74 mW/cm² (applied UV fluence: 20,664 mJ/cm²) and 5.68 mW/cm² (applied UV fluence: 20,448 mJ/cm²). The degradation by-products using LC-MS/MS and ACD/MS Fragmenter software were identified. During UV-B photolysis, eight by-products (m/z 414.3, 417.3, 709.6, 428.9, 608.6, 847.5, 807.4, and 823.6) were newly identified. In contrast, eleven MC-LR by-products (m/z 707.4, 414.7, 429.3, 445.3, 608.6, 1052.0, 313.4, 823.6, 357.3, 245.2, and 805.7) were newly confirmed during the UV-B/ H₂O₂ process. Most by-products of MC-LR had low m/z values than m/z value of MC-LR. Based on the identified by-products and their peak area patterns, potential degradation mechanisms and pathways were proposed. The bond cleavage and free electron pair transfer reactions containing nitrogen atoms were the major reactions during UV-B photolysis. The reaction with an OH radical and addition reaction with other by-

products were identified as additional reaction pathways during the UV-B/H₂O₂ process.

This study provides important information for removing MC-LR by UV-B photolysis and UV-B/H₂O₂ processes. In addition, this study offers method support for MC-LR degradation by-products identification. Our results imply that, the UV-B/H₂O₂ process can be effectively applied in WTPs by removing MC-LR, but, the toxicity studies of their by-products should be needed.

5. References

- Al Monami F., Smith D. W., El-Din M. G. 2008. Degradation of cyanobacteria toxin by advanced oxidation processes. *J. Hazard. Mater.* 150 (2), 238-249.
- An J., Carmichael W. W. 1994. Use of a colorimetric protein phosphatase inhibition assay and enzyme linked immunosorbent assay for the study of microcystins and nodularins. *Toxicon* 32 (12), 1495-1507.
- Anderson J., Han C., O'Shea K., Dionysiou D. D. 2014. Revealing the degradation intermediates and pathways of visible light-induced NF-TiO₂ photocatalysis of microcystin-LR. *Appl. Catal., B* 154, 259-266.
- Antoniou M. G., Shoemaker J. A., Armah A., Dionysiou D. D. 2008. LC/MS/MS structure elucidation of reaction intermediates formed during the TiO₂

- photocatalysis of microcystin-LR. *Toxicon* 51 (6), 1103-1118.
- Antoniou M. G., Shoemaker J. A., Cruz A. A. D. L., Dionysiou D. D. 2008. Unveiling new degradation intermediates/pathways from the photocatalytic degradation of microcystin-LR. *Environ. Sci. Technol.* 42 (23), 8877-8883.
- Bigham D. L., Hoyer M. V., Canfield Jr D. E., 2009. Survey of toxic algal (microcystin) distribution in Florida lakes. *Lake and Reservoir Management* 25 (3), 264-275.
- Chang J., Chen L., Wang Z., Shen J. M., Chen Q., Kang J., Yang L, Liu X. W., Nie C. X. 2014. Ozonation degradation of microcystin-LR in aqueous solution: Intermediates, byproducts and pathways. *Water Res.* 63, 52-61.
- Chow C. W., Drikas M., House J., Burch M. D., Velzeboer R. M. 1999. The impact of conventional water treatment processes on cells of the cyanobacterium *Microcystis aeruginosa*. *Water Res.* 33 (15), 3253-3262.
- Colonna G. M., Caronna T., Marcandalli B. 1999. Oxidative degradation of dyes by ultraviolet radiation in the presence of hydrogen peroxide. *Dyes Pigm.* 41 (3), 211-220.
- Croll. B., Hart. J. 1996. Algal toxins and customers. In UKWIR-AWWARF Technology Transfer Conference. Philadelphia, 14-16.
- Dai M., Xie P., Liang G., Chen J., Lei H. 2008. Simultaneous determination of

- microcystin-LR and its glutathione conjugate in fish tissues by liquid chromatography–tandem mass spectrometry. *J. Chromatogr. B* 862 (1), 43-50.
- Dawson R. 1998. The toxicology of microcystins. *Toxicon* 36 (7), 953-962.
- Feurstein D., Stemmer K., Kleinteich J., Speicher T., Dietrich D. R. 2011. Microcystin congener-and concentration-dependent induction of murine neuron apoptosis and neurite degeneration. *Toxicological sciences*. Kfr342.
- Gulldge B. M., Aggen J. B., Huang H., Naim A. C., Carmberlin A. R. 2002. The microcystins and nodularins: cyclic polypeptide inhibitors of PP1 and PP2A. *Curr. Med. Chem.* 9 (22), 1991-2003.
- Gurbuz F., Codd G. A. 2008. Microcystin removal by a naturally-occurring substance: pumice. *Bull. Environ. Contam. Toxicol.* 81 (3), 323-327.
- Graham J. L., Loftin K. A., Meyer M. T., Ziegler. A. C. 2010. Cyanotoxin mixture and taste-and-odor compounds in cyanobacterial blooms from the Midwestern United States. *Environmental science & technology*. 44 (19), 7361-7368.
- He J., Chen J., Xie P., Zhang D., Li G., Wu L, Zhang W., Guo X., Li S. 2012. Quantitatively evaluating detoxification of the hepatotoxic microcystins through the glutathione and cysteine pathway in the cyanobacteria-eating bighead carp. *Aquat. Toxicol.* 116, 61-68.
- He X., Armah A., Hiskia A., Kaloudis T., O'Shea K., Dionysiou D. D. 2015.

- Destruction of microcystins (cyanotoxins) by UV-254 nm-based direct photolysis and advanced oxidation processes (AOPs): Influence of variable amino acids on the degradation kinetics and reaction mechanisms. *Water Res.* 74, 227-238.
- He X., Pelaez M., Westrick J. A., O'Shea K. E., Hiskia A., Triantis T., Kaloudis T., Stefan M. I., Cruz A. A. D. L., Dionysiou D. D. 2012. Efficient removal of microcystin-LR by UV-C/H₂O₂ in synthetic and natural water samples. *Water Res.* 46 (5), 1501-1510.
- Huang W. J., Cheng B. L., Cheng Y. L. 2007. Adsorption of microcystin-LR by three types of activated carbon. *J. Hazard. Mater.* 141 (1), 115-122.
- Jacobs L. C., Peralta-Zamora P., Camopos F. R, Pontarolo R. 2013. Photocatalytic degradation of microcystin-LR in aqueous solutions. *Chemosphere* 90 (4), 1552-1557.
- Kaya K., Sano T. 1998. A photodetoxification mechanism of the cyanobacterial hepatotoxin microcystin-LR by ultraviolet irradiation. *Chem. Res. Toxicol.* 11 (3), 159-163.
- Keijola A. M., Himberg K., Esala A. L., Sivonen K., Hiis-Virta L. 1988. Removal of cyanobacterial toxins in water treatment processes: Laboratory and pilot-scale experiments. *Toxicity assessment* 3 (5), 643-656.
- Lanaras T., Cook C. M., Eriksson J. E., Meriluoto J. A. O., Hotokka M. 1991.

- Computer modelling of the 3-dimensional structures of the cyanobacterial hepatotoxins microcystin-LR and nodularin. *Toxicon* 29 (7), 901-906.
- Legrini O., Oliveros E., Braun A. M. 1993. Photochemical processes for water treatment. *Chem. Rev.* 93 (2), 671-698.
- McElhiney J., Lawton L. A. 2005. Detection of the cyanobacterial hepatotoxins microcystins. *Toxicol. Appl. Pharmacol.* 203 (3), 219-230.
- Merel S., LeBot B., Clément M., Seux R., Thomas O. 2009. MS identification of microcystin-LR chlorination by-products. *Chemosphere* 74 (6), 832-839.
- Merel S., Walker D., Chicana R., Snyder S., Baures E., Thomas O. 2013. State of knowledge and concerns on cyanobacterial blooms and cyanotoxins. *Environ. Int.* 59, 303-327.
- Qiao R. P., L, N., Qi X. H., Wang Q. S., Zhuang Y. Y. 2005. Degradation of microcystin-RR by UV radiation in the presence of hydrogen peroxide. *Toxicon*, 45(6), 745-752.
- Rajaratnam R. 1992. Electron transfer chain reactions in systems containing carbon-nitrogen double bonds.
- Richard J., Boergers A., vom Eyser C., Bester K., Tuerk J. 2014. International Journal of Hygiene and Environmental Health. *International Journal of Hygiene and Environmental Health*, 217, 506-514.

- Rinehart K. L., Namikoshi M., Choi B.W. 1994. Structure and biosynthesis of toxins from blue-green algae (cyanobacteria). *J. Appl. Phycol.* 6 (2), 159-176.
- Rinta-Kanto J. M., Konopko E. A., DeBruyn J. M., Bourbonniere R. A., Boyer G. L., Wilhelm S. W. 2009. Lake Erie Microcystis: relationship between microcystin production, dynamics of genotypes and environmental parameters in a large lake. *Harmful Algae* 8 (5), 665-673.
- Rodrigues M. A., Reis M. P., Mateus M. C. 2013. Liquid chromatography/negative electrospray ionization ion trap MS2 mass spectrometry application for the determination of microcystins occurrence in Southern Portugal water reservoirs. *Toxicon*. 74, 8-18.
- Ulstrup J., Jortner J. 1975. The effect of intramolecular quantum modes on free energy relationships for electron transfer reactions. *J. Chem. Phys.* 63 (10), 4358-4368.
- United States Environmental Protection Agency 2012. Cyanobacteria and Cyanotoxins: Information for Drinking water systems. Office of Water 4304T EPA-810F11001.
- Weng D., Lu Y., Wei Y., Liu Y., Shen P. 2007. The role of ROS in microcystin-LR-induced hepatocyte apoptosis and liver injury in mice. *Toxicology* 232 (1), 15-23.
- WHO 2003. Cyanobacterial toxins: Microcystin-LR in drinking water. Background

document for preparation of WHO Guidelines for drinking-water quality.
Geneva, World Health Organization WHO/SDE/WSH/03.04/57.

Xue Q., Steinman A. D., Su X., Zhao Y., Xie L., 2016. Temporal dynamics of microcystins in *Limnodrilus hoffmeisteri* a dominant oligochaete of hypereutrophic Lake Taihu, China. *Environmental Pollution*. 213, 585-593.

Zhao Y., Xie L., Yan Y. 2015. Microcystin-LR impairs zebrafish reproduction by affecting oogenesis and endocrine system. *Chemosphere* 120, 115-122.

Zong W., Sun F., Sun X. 2013. Evaluation on the generative mechanism and biological toxicity of microcystin-LR disinfection by-products formed by chlorination. *J. Hazard. Mater.* 252, 293-299.

Zong W., Sun F., Pei H., Hu W., Pei R. 2015. Microcystin-associated disinfection by-products: the real and non-negligible risk to drinking water subject to chlorination. *Chem. Eng. J.* 279, 498-506.

국문초록

최근 기후 변화로 인해 이상 고온, 강수량 감소, 일조량 증가 현상이 빈번하게 일어남에 따라 상수원에서 남조류가 대량 증식하고 있다. 남조류의 대량 발생은 특히 남조류 중 독성을 가진 마이크로시스틴-LR을 생성 및 분비하여 경제 및 공중 보건학적으로 심각한 문제를 야기하고 있다. 이러한 이유로 수계 내 존재하는 마이크로시스틴-LR의 모니터링 및 처리에 관한 연구는 광범위하게 다루어졌으나 처리 후 부산물에 대한 연구는 많이 미흡한 실정이다. 마이크로시스틴-LR은 기존 처리 방법을 적용할 때 거의 제거가 되는 것으로 알려져 있으나 마이크로시스틴-LR은 분자량이 크기에 다양한 제거부산물이 생성될 수 있으며 이 부산물들은 잠재적인 위험을 가지고 있을 가능성이 존재한다. 그러므로 본 연구에서는 마이크로시스틴-LR의 처리 부산물을 규명하고 분해경로를 제시하는 방향으로 진행하였다. 자외선 광분해와 자외선/과산화수소 반응을 통한 마이크로시스틴-LR의 분해 메커니즘과 부산물 생성을 평가하기 위해 두 반응을 비교하여 분해 부산물을 규명하고 분해경로를 제시하였다. 두 반응에서의 제거 반응은 모두 유사 1차 반응을 따랐으며, 처리 부산물들은 LC-MS/MS를 이용하여 규명하였다. 자외선 광반응에서는 총 8개의 분해 부산물을 발견할 수 있었고 이는 결합의

분해와 질소원자에서의 자유전자쌍의 전이 메커니즘을 따르는 것으로 사료되었다. 자외선/과산화수소 반응에서는 총 11개의 분해 부산물을 발견하였으며 이 중 2개의 분해 부산물은 자외선 광반응에서 발견된 부산물과 일치하는 것으로 나타났다. 자외선/과산화수소 반응에서의 메커니즘은 자외선 광반응과 같은 결합의 분해와 질소원자에서의 자유전자쌍의 전이 메커니즘 외에 OH 라디칼 첨가 및 규명된 두 부산물의 결합 메커니즘으로 사료된다.

핵심어: 조류독소, 마이크로시스틴-LR, 광분해, 자외선/과산화수소, 부산물